MNRAS **442,** 2586–2599 (2014) doi:10.1093/mnras/stu999

GRB 051008: a long, spectrally hard dust-obscured GRB in a Lyman-break galaxy at $z \approx 2.8$★

A. A. Volnova,[1]† A. S. Pozanenko,[1] J. Gorosabel,[2] D. A. Perley,[3,4] D. D. Frederiks,[5] D. A. Kann,[6,7] V. V. Rumyantsev,[8] V. V. Biryukov,[8,9] O. Burkhonov,[10] A. J. Castro-Tirado,[2] P. Ferrero,[11,12] S. V. Golenetskii,[5] S. Klose,[6] V. M. Loznikov,[1] P. Yu. Minaev,[1] B. Stecklum,[6] D. S. Svinkin,[5] A. E. Tsvetkova,[5] A. de Ugarte Postigo[2,13] and M. V. Ulanov[5]

[1]*Space Research Institute, 84/32 Profsoyuznaya Street, Moscow 117997, Russia*
[2]*Instituto de Astrofísica de Andalucía del Consejo Superior de Investigaciones Cientificas (IAA-CSIC), Camino Bajo de Huetor 50, E-18080 Granada, Spain*
[3]*Department of Astronomy, California Institute of Technology, MC 249-17, 1200 East California Blvd., Pasadena, CA 91125, USA*
[4]*Hubble fellow*
[5]*Ioffe Physical-Technical Institute, Politekhnicheskaya 26, St. Petersburg 194021, Russia*
[6]*Thüringer Landessternwarte Tautenburg,Sternwarte 5, D-07778 Tautenburg, Germany*
[7]*Max-Planck-Institut für extraterrestrische Physik, Giessenbachstraße 1, D-85748 Garching, Germany*
[8]*Crimean Astrophysical Observatory, Taras Shevchenko National University of Kyiv, Nauchny, UK-98409 Crimea, Ukraine*
[9]*Crimean Laboratory of the Sternberg Astronomical Institute, Nauchny, UK-98409 Crimea, Ukraine*
[10]*Institute of Astronomy, Academy of Sciences of Uzbekistan, Tashkent, Uzbekistan*
[11]*Instituto de Astrofisica de Canarias (IAC), E-38200 La Laguna, Tenerife, Spain*
[12]*Departamento de Astrofisica, Universidad de La Laguna (ULL), E-38205 La Laguna, Tenerife, Spain*
[13]*Dark Cosmology Centre, Niels Bohr Institute, University of Copenhagen, Juliane Maries Vej 30, DK-2100 Copenhagen, Denmark*

Accepted 2014 May 16. Received 2014 May 8; in original form 2014 March 5

ABSTRACT

We present observations of the dark gamma-ray burst GRB 051008 provided by *Swift*/BAT, *Swift*/XRT, Konus-*WIND*, *INTEGRAL*/SPI-ACS in the high-energy domain and the Shajn, *Swift*/UVOT, Tautenburg, NOT, Gemini and Keck I telescopes in the optical and near-infrared bands. The burst was detected only in gamma- and X-rays and neither a prompt optical nor a radio afterglow was detected down to deep limits. We identified the host galaxy of the burst, which is a typical Lyman-break galaxy (LBG) with *R*-magnitude of 24.06 ± 0.10 mag. A redshift of the galaxy of $z = 2.77^{+0.15}_{-0.20}$ is measured photometrically due to the presence of a clear, strong Lyman-break feature. The host galaxy is a small starburst galaxy with moderate intrinsic extinction ($A_V = 0.3$) and has a star formation rate of $\sim 60\,M_\odot\ yr^{-1}$ typical for LBGs. It is one of the few cases where a GRB host has been found to be a classical LBG. Using the redshift we estimate the isotropic-equivalent radiated energy of the burst to be $E_{iso} = (1.15 \pm 0.20) \times 10^{54}$ erg. We also provide evidence in favour of the hypothesis that the darkness of GRB 051008 is due to local absorption resulting from a dense circumburst medium.

Key words: gamma-ray burst: individual: dark – galaxies: distances and redshifts – galaxies: high-redshift – galaxies: photometry.

1 INTRODUCTION

Cosmic gamma-ray bursts (GRBs) are among the most powerful events in the Universe. A detection of a GRB is expected to be followed by the detection of an afterglow in other spectral ranges: X-ray, optical, and radio emissions. Presently, a large number of ground-based robotic telescopes search for optical afterglows rapidly after GRBs have occurred. Also, on-board the dedicated *Swift* space observatory (Gehrels et al. 2004), the UltraViolet/Optical Telescope (UVOT; Roming et al. 2005a) is used for rapid follow-up of UV and optical afterglows. However, it is now clear that for a substantial fraction of events (from 20 per cent; Cenko et al. 2009; Greiner et al. 2011, to 35 per cent, Melandri et al. 2012) we are currently unable to detect any optical afterglow, even with rapid follow-up within the first minutes after the GRB (see also Fynbo et al. 2001; Lazatti, Covino & Ghisellini 2002).

★Based on observations made with the Nordic Optical Telescope, operated on the island of La Palma jointly by Denmark, Finland, Iceland, Norway, and Sweden, in the Spanish Observatorio del Roque de los Muchachos of the Instituto de Astrofisica de Canarias.

†E-mail: alinusss@gmail.com

Faintness or the complete lack of an optical afterglow (OA) may be caused by different factors. Most prosaically, a failure to detect the OA may be due to the low limiting magnitude of the observations, such as when only small robotic telescopes observe the GRB position early on (in contrast to larger rapid follow-up telescopes; see Greiner et al. 2011).

A possible factor for a GRB to be dark is the immediate neighbourhood of its source. The 'extinction scenario' (Taylor et al. 1998) assumes that the emission of the OA is strongly absorbed in the host galaxy. Moreover, the GRB source may be surrounded by a dense circumburst medium (Paczynski 1998; Galama & Wijers 2001).

Another potential origin of dark bursts is a high redshift. Emission with wavelengths shorter than $912(1+z)$ Å in the observer frame is efficiently absorbed due to the Lyman-cutoff when it passes through the intergalactic medium (Lamb & Reichart 2000).[1] For $z \geq 4$, this Lyman drop-out falls into the R_C band in the optical in which most rapid searches for GRB afterglows are carried out. Such GRBs can only be localized through rapid, deep near-infrared (NIR) follow-up, e.g. as in the case of GRB 080913 (Greiner et al. 2009; Pérez-Ramírez et al. 2010).

To determine whether the burst is genuinely dark, due to some physical factors rather than to an inefficient search, it is useful to compare the observed optical/near-IR detections or upper limits with the values expected from the brightness of the X-ray afterglow. This approach is based on the standard fireball model (Sari, Piran & Narayan 1998), where the afterglow spectrum produced by the synchrotron radiation follows the simple power law (PL) $F_\nu \sim \nu^{-\beta}$. Jakobsson et al. (2004) proposed to define dark bursts using an optical to X-ray spectral index $\beta_{\rm OX} < 0.5$, since in log space it is the shallowest expected slope of the synchrotron spectrum in the standard afterglow model. Alternatively, van der Horst et al. (2009) use the value of the X-ray spectral index $\beta_{\rm X}$, assuming for the definition of dark bursts the condition $\beta_{\rm OX} - \beta_{\rm X} < 0.5$.

Finally, the burst may be intrinsically faint and the low optical luminosity of its OA may be due to a low density of the interstellar medium into which the relativistic outburst of the GRB propagates (Sari et al. 1998, note that in this case a GRB may not be dark according to the Jakobsson criterion, as it may also have a very faint X-ray afterglow).

Long GRBs are known to be linked to the deaths of massive stars, and hence to star formation activity (Jimenez & Piran 2013). As a result, one may expect some GRBs to be located in dusty environments, with high extinction values along the lines of sight towards the bursts, or even high bulk extinction in the host galaxies. Melandri et al. (2008) found that about 50 per cent of *Swift* dark bursts show evidence of a mild extinction. Further studies by Perley et al. (2009) showed that the majority of dark bursts require $A_V^{\rm host} \geq 1$ mag, with a few cases reaching ∼2–6 mag. There are many notable examples of highly extinguished events: GRB 980828 (Djorgovski et al. 2001); GRB 051022 (Castro-Tirado et al. 2007); GRB 061222A (Perley et al. 2009); GRB 070306 (Jaunsen et al. 2008); GRB 070521 (Perley et al. 2009); GRB 080325 (Hashimoto et al. 2010); GRB 080607 (Chen et al. 2010; Perley et al. 2011); GRB 090417B (Holland et al. 2010); GRB 100621A (Greiner et al. 2013); GRB 110709B and GRB 111215A (Zauderer et al. 2013).

The study of properties of host galaxies is one of the tools for investigating the environment in which the GRBs form (e.g. Savaglio, Glazebrook & Le Borgne 2009). Recent research on large populations of dark-GRB host galaxies has shown that, generally, they do not differ from the host galaxies of GRBs that suffer from little dust extinction (Perley et al. 2009), with the 'darkness' being mostly due to local extinction around the progenitor in galaxies of low to medium redshifts. But one can note that some very dark GRBs trace a population of extremely red host galaxies (Hunt et al. 2011; Rossi et al. 2012; Svensson et al. 2012), whereas highly extinguished (but still detected) GRB afterglows are preferentially linked with more massive host galaxies (Krühler et al. 2011). The host galaxies of dark GRBs in general have large star formation rate (SFRs; Perley et al. 2013).

Redshifts of detected host galaxies vary in a wide range from $z = 0.0085$ (GRB 980425; Tinney et al. 1998) to $z = 4.667$ (GRB 100219A; Thöne et al. 2013) with a median value of $z_{\rm host}$ about 1.4.[2] About 20 per cent of discovered GRB host galaxies lie at redshifts more than 2.5. The search for galaxies with $z \geq 2.5$ and their spectroscopic observations is a non-trivial problem. In these cases techniques of photometric redshift estimation are useful. For example, the Lyman limit of hydrogen at 912 Åin the rest frame of a galaxy helps to find ordinary starburst galaxies at $z \sim 3$ and at higher redshifts to identify Lyman break galaxies (LBGs). But to date there were only a few associations between GRBs and LBGs (Odewahn et al. 1998; Malesani et al. 2013). Also if GRBs trace star-formation one should expect that a typical GRB host galaxy at $z > 2.5$ will be under-luminous and fall below L^* of the LBG luminosity function (Jakobsson et al. 2005a; Fynbo et al. 2008). In the case of dark bursts the discovery of the host galaxy is often the only way to determine the distances to these sources and to try to obtain an insight into their nature (e.g. Jakobsson et al. 2012; Krühler et al. 2012a).

In this paper we determine and discuss properties of GRB 051008 and its host galaxy. We present detailed parameters of the prompt γ-ray emission observed by Konus-*WIND* in the energy range up to 14 MeV which is essential for determining the physical parameters $E_{\rm p}$ and $E_{\rm iso}$. We also report new observations of the host galaxy which were not published earlier in preliminary studies (Volnova et al. 2010a, 2010b). In particular these observations in U, g', R, I, and Z bands provided by the Keck I telescope, in K' band provided by the Gemini North telescope, and ultra-violet observations provided by *Swift*/UVOT, helped us to determine a secure photometric redshift of the galaxy. In the paper we use the following notations and conventions: time-decay, photon, and spectral indices are indicated with α, Γ, and β, following the standard convention $t^{-\alpha}$, $N_{\rm ph}^{-\Gamma}$, and $\nu^{-\beta}$, respectively. We use the following cosmological parameters $H_0 = 71$ km s^{-1} Mpc^{-1}, $\Omega_{\rm M} = 0.27$, $\Omega_\Lambda = 0.73$ and cosmological calculations of Ned Wright's Cosmology Calculator (Wright 2006). If not stated otherwise, all errors represent one standard deviation, and upper limits are three standard deviations for the parameter of interest.

2 THE GAMMA-RAY BURST GRB 051008

2.1 Detection of the burst

The gamma-ray burst GRB 051008 was detected by the BAT telescope of the *Swift* space observatory at 16:33:21 UT on 2005 October 8 (Marshall et al. 2005). The burst occurred during a telemetry downlink transmission and that is why the corresponding alert was not received by the BACODINE γ-ray alert network[3] until 10 min after the event. The spacecraft did not slew to the burst immediately

[1] At higher redshifts the Lyα forest becomes effectively opaque causing the break to be at $1217(1+z)$ Å.

[2] http://www.grbhosts.org/

[3] S. Barthelmy, http://gcn.gsfc.nasa.gov/

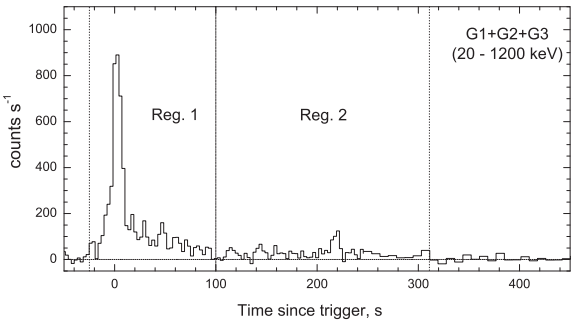

Figure 1. An overview of the Konus-*WIND* light curve. The background-subtracted time history in the G1+G2+G3 bands is presented. The fluence calculation intervals are tagged as *Reg. 1* and *Reg. 2*.

because of the Earth-limb observing constraint. This condition also prevented *Swift*/BAT from recording all gamma radiation from the event (see Section 2.2). This burst was also detected at 16:33:18 UT by the WAM γ-ray monitor on-board the *Suzaku* observatory and had a duration of 48 s in the energy range from 100 keV to 2 Mev. The burst spectrum in this energy range can be fitted fairly well by a CPL model with $dN/dE \sim E^{\Gamma} e^{-E/E_c}$ with photon index $\Gamma = -1.24 \pm 0.15$, and a cut-off energy of $E_c = 1535^{+1419}_{-561}$ keV (Ohno et al. 2005).

GRB 051008 was also recorded by Konus-*WIND* (see Section 2.2), as well as the SPI-ACS detector on-board *INTEGRAL* observatory (see Section 2.3), and the Mars Observer spacecraft.[4]

2.2 Konus-*WIND* observations

GRB 051008 triggered detector S2 of the Konus-*WIND* γ-ray spectrometer (Aptekar et al. 1995) at T_0 = 16:33:21 UT. As derived from the *WIND* spacecraft ephemerides and the *Swift* localization of the GRB source, the corresponding Earth-crossing time is $T_\oplus = T_0+2.8$ s.

In the triggered mode, the burst time histories are recorded by the instrument in three energy bands: G1 (20–80 keV), G2 (80–300 keV), and G3 (300–1200 keV). The measurement started from 0.5 s before and up to 229.6 s after the spacecraft trigger, with a time resolution varying from 2 ms up to 256 ms. The time history of the burst is also available from the instrument's waiting-mode data, which are recorded up to T_0+250 s in the same energy bands with 2.944 s time resolution. A search for a possible precursor to the burst was performed using this data set, with no statistically significant positive result up to $T_0 - 1500$ s.

As observed by Konus-*WIND*, the burst light curve shows a multi-peaked hard-spectrum pulse which starts at $\sim T_0 - 25$ s and decays to $\sim T_0+100$ s (Fig. 1). Additional information about the burst light curve after T_0+250 s can be extracted from the multichannel spectra which are measured up to T_0+490 s. The analysis of these data shows that the γ-ray emission continues, mostly in the soft G1 band, up to $\sim T_0+310$ s. The total burst duration T_{100} = 246.1 s was determined at the 5σ level in the 20–1200 keV band. The corresponding value of T_{90} is 214 ± 30 s and T_{50} = 48 ± 4 s.

During the burst the instrument measured 64 multichannel energy spectra covering two partially overlapping energy ranges: PHA1 (20–1200 keV) and PHA2 (0.4–14 MeV). The spectral analysis was performed using XSPEC V12.5 (Arnaud 1996) by applying three spectral models. The first one is a simple PL: $f(E) \propto E^{\Gamma}$ where Γ is the PL photon index. The second model is a PL with an exponential cut-off, parametrized as E_{peak}: $f(E) \propto E^{\Gamma} exp(-(2+\Gamma)E/E_{peak})$ where E_{peak} is the peak energy in the νF_ν spectrum. The third model is the Band function (Band et al. 1993): $f(E) \propto E^{\Gamma} exp(-(2+\Gamma)E/E_{peak})$ for $E < E_{peak}(\Gamma - \Gamma_2)/(2+\Gamma)$, and $f(E) \propto E^{\Gamma_2}$ for $E \geq E_{peak}(\Gamma - \Gamma_2)/(2+\Gamma)$ where Γ_2 is the photon index in the higher energy band.

A summary of the Konus-*WIND* spectral fits is presented in Table 1. The spectrum of the brightest part of the burst (measured from T_0 to T_0 +8.192 s) is best fitted in the 20–14000 keV energy range with the Band model (χ^2 = 101/88 dof) (see Fig. 2). The CPL function yields a fit result of similar quality (χ^2 = 105/89 dof). For both mentioned models relatively high values of E_{peak} ∼ 700 keV are obtained, placing this burst among the hardest of the Konus-*WIND* long GRBs. The time-integrated spectrum of the main part of the GRB (measured from T_0 to $T_0+98.3$ s) is also best fitted by the Band function with $E_{peak} = 307^{+195}_{-101}$ keV (χ^2 = 97/96 dof). Considering a spectrum of the final part of the burst (from T_0 +98.3 to T_0 +311.3 s) the only model for which the fit parameters are constrained is a simple PL function yielding the photon index Γ close to −2 (χ^2 = 117/98 dof).

Based on the results of the spectral analysis the observed burst energetics parameters such as energy fluence (Table 2) and peak energy flux are calculated. The latter value reaches $F_{max} = (7.0 \pm 0.7) \times 10^{-6}$ erg cm^{-2} s^{-1} in a 64 ms time interval starting at $T_0+1.1$ s. The total energy fluence of the burst amounts to $S = (6.5 \pm 1.1) \times 10^{-5}$ erg cm^{-2}. Both values are measured in the 20 keV–10 MeV energy range, standard for calculations of the Konus-*WIND* GRB energetics, and the quoted errors are at the 90 per cent confidence level.

It is possible to consider the GRB time history in the three energy bands (G1, G2, G3) as a series of three-channel energy spectra. In this case the spectral variability of the burst can be studied on a faster time-scale (Mazets et al. 2001; Ulanov et al. 2005). We applied this method to the GRB 051008 light curve in order to obtain the fine temporal behaviour of the CPL spectral model parameters E_{peak} and Γ during the brightest phase of the burst. As a result (Fig. 3) clear evidence of spectral variability in the form of a hardness–intensity correlation is obtained (particularly between E_{peak} and the light curves above 80 keV).

We also examined the spectral lag τ_{lag} using the cross-correlation function (CCF) between the light curves in two energy bands (Norris, Marani & Bonnell 2000; Band 1997). After calculating the CCF as a function of the lag τ_{lag} we obtained the peak value of τ_{lag} by fitting it with a fourth-degree polynomial. The resulting values of τ_{lag} between the G1, G2, and G3 light curves in different combinations are listed in Table 3. As one can see none of these values differs from zero by more than one standard deviation and thus a negligible spectral lag is evident (see also Section 2.3). This result places GRB 051008 among the 17 per cent of zero-lag events of the Konus-*WIND* sample of ∼950 long GRBs with well-determined spectral lags (Svinkin et al., in preparation).

2.3 *INTEGRAL* observations

The burst was detected by the SPI-ACS detector on-board the *INTEGRAL* observatory at 16:33:12 UT.[5] The burst position was $\theta = 86^\circ$ off the axis of the aperture telescopes. The SPI-ACS continuously records count rates in a single wide energy band ∼(80–10000) keV

[4] http://www.ssl.berkeley.edu/ipn3/masterli.txt

[5] http://www.isdc.unige.ch/INTEGRAL/ibas/cgi-bin/ibasacsweb.cgi/?trigger = 2005-10-08T16-33-12.1588-07660-00007-0

Table 1. Summary of Konus-*WIND* spectral fits in 0.02–14 MeV energy range.

Time interval (s)	Spectral model	Γ	E_{peak} (keV)	Γ_2	χ^2/dof
Central part (T_0 to T_0+8.2)	Band	−0.95 (−0.10,+0.12)[a]	660 (−161,+183)	−2.34 (−1.23,+0.24)	101/88
	CPL	−1.00 (−0.08,+0.09)	770 (−123,+162)	–	105/89
	PL	−1.46 (−0.02,+0.02)	–	–	306/90
Main pulse (T_0 to T_0+98)	Band	−0.75 (−0.28,+0.40)	307 (−101,+195)	−2.10 (−0.59,+0.20)	97/96
	CPL	−1.06 (−0.15,+0.18)	563 (−157,+291)	–	101/97
	PL	−1.51 (−0.04,+0.04)	–	–	185/99
Tail (T_0+98 to T_0+311)	PL[b]	−1.97 (−0.32,+0.39)	–	–	117/98

[a]All the quoted errors are at the 90 per cent confidence level.
[b]In this region parameters of the CPL and Band models are not constrained.

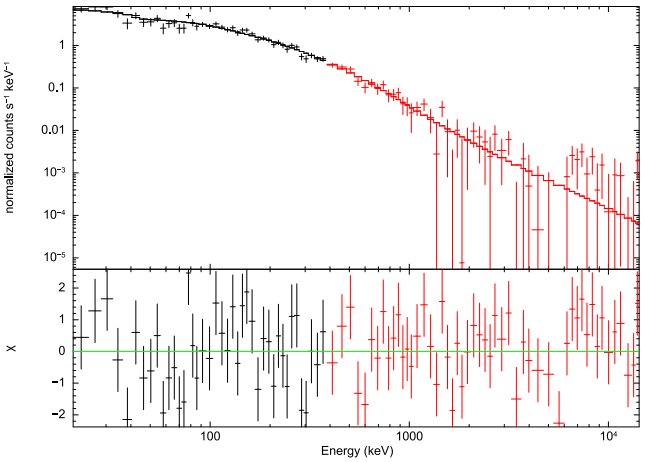

Figure 2. The Konus-*WIND* energy spectrum measured from T_0 to T_0+8.2 s and its fit with the Band function (see Table 1 for details).

Table 2. GRB 051008 energy fluence measured with Konus-*WIND*.

Time interval (s)	Spectral range (keV)	Fluence, (10^{-5} erg cm^{-2})
Region 1[a] (T_0 − 25 to T_0+98)	20–14 000	5.9 ± 1.0[b]
Region 2 (T_0+98 to T_0+311)	20–14 000	0.8 ± 0.5
Whole burst (T_0 − 25 to T_0+311)	20–14 000	6.7 ± 1.1

[a]The fluence for the pre-trigger part (from T_0 − 25 s to T_0) is estimated using a product of the count fluence for this part and the conversion factor from a count fluence to an energy fluence using the spectral information of the time-averaged spectrum.
[b]All the quoted errors are at the 90 per cent confidence level.

with a time resolution of 50 ms (von Kienlin et al. 2003). Owing to the large size of the SPI-ACS detector (geometrical surface area is 5250 cm^2 at the $\theta = 90$) significant (3σ) emission was detected up to 800 s after the burst trigger (Fig. 4). We again searched for a possible precursor but did not find one in the range of T_0 − 1500 s. The T_{90} in the energy band of SPI-ACS is 535 ± 40 s.

Using the original time resolution we searched for a possible periodicity of the whole light curve. No significant periodicity was found on time-scales from 0.1 to 20 s. We also investigated the power spectrum of the main peak of the burst in the time interval

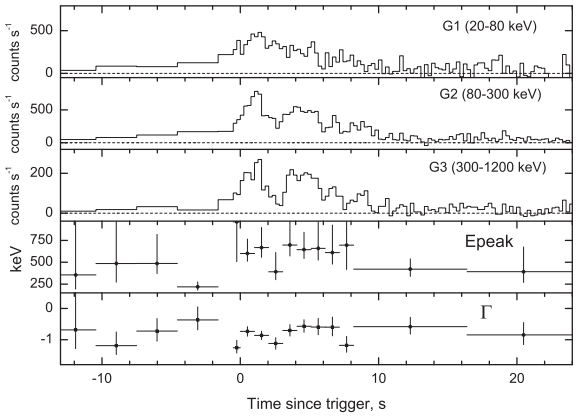

Figure 3. Spectral evolution of the prompt γ-ray emission during the main phase of the burst. Background-subtracted light curves in three energy bands (G1, G2, G3) are shown, along with the temporal behaviour of the CPL spectral model parameters E_{peak} and Γ.

Table 3. Spectral lag between Konus-*WIND* light curves in the time interval [0–10 s.]

Light curves	Time-scale (ms)	τ^a_{lag} (s)
G3–G1	256	−0.2 ± 0.3[b]
G2–G1	256	−0.16 ± 0.14
G3–G2	64	0.06 ± 0.06

[a]In this table positive spectral lag means that the spectrum has hard-to-soft evolution.
[b]All the quoted errors are at 1σ level.

[10–20] s after trigger (see inset in Fig. 4). The power density spectrum (PDS) can be fitted by a single PL with index of −2.06 ± 0.09 up to 7 Hz. The PL index significantly differs from the index ∼1.6 of averaged PDS obtained for long GRBs (Beloborodov, Stern & Svensson 2000; Pozanenko & Loznikov 2000).

GRB 051008 is a good example of a multi-peak event. Using SPI-ACS data and technique developed early (Minaev et al. 2014) we found at least 10 separated pulses which fit the light curve fairly well (Fig. 4b). We cannot investigate the spectral lag of the separate pulses due to heavy overlap of the pulses. There was found the existence of the lag versus pulse duration correlation (Hakkila et al. 2007; Minaev et al. 2013, 2014), i.e. the shorter pulse, the smaller spectral lag corresponds to the pulse. Its multi-peak structure of short duration pulses composing the main body of a burst light

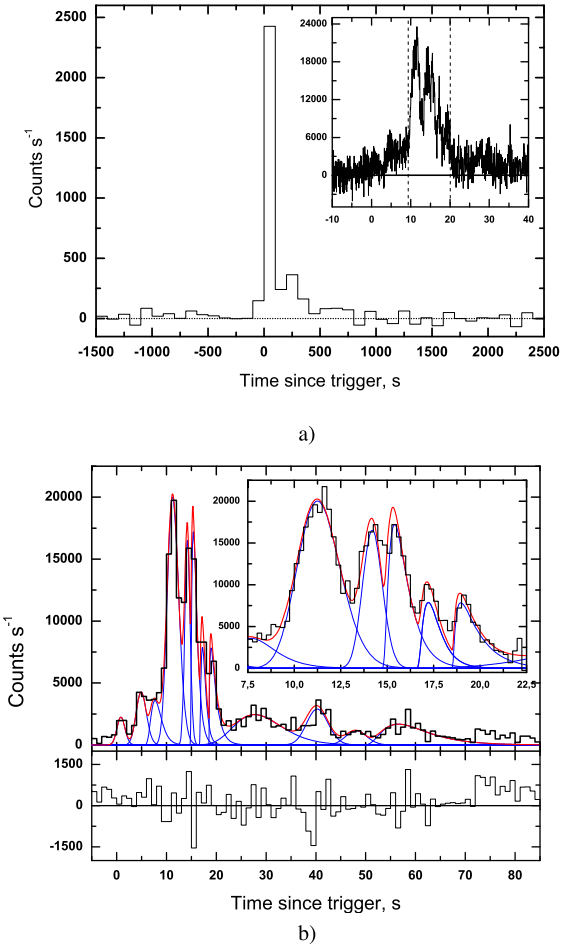

Figure 4. (a) Background-subtracted light curve of GRB 051008 obtained by the *INTEGRAL*/SPI-ACS in the energy band ∼80 keV–10 MeV. Here, the original light curve with a time resolution of 50 ms has been re-binned into 100 s bins. Inset: the light curve of the main peak of the burst; the dashed lines denote the time interval for the PDS calculation (see Section 2.3). (b) top panel: the light curve at 1 s time resolution fit with a number of single pulses; (b), bottom panel: residuals.

curve could be the underlying nature of a negligible lag of the GRB 051008 as a whole (see Table 3 and Fig. 4).

Since the lag of the whole burst is not an additive function of the lag of separate pulses even superposition of pulses with positive lags may result in a negative lag of a complex of superimposed pulses (Minaev et al. 2014). This is another plausible reason of the negligible lag of the GRB 051008.

2.4 *Swift*/XRT observations

The XRT X-ray telescope (Burrows, Hill & Nousek 2005) on-board the *Swift* space observatory began observing the region of the burst at 17:23:52 UT, i.e. 50 min after the BAT trigger. The XRT detected the fading X-ray source (Perri, Capalbi & Burrows 2005) which was identified as the X-ray afterglow of the burst. Butler (2007) provided an on-ground SDSS-enhanced position of the X-ray afterglow at RA $= 13^{\rm h}31^{\rm m}29\overset{\rm s}{.}55$, Dec. $= +42^{\circ}05'53\overset{''}{.}3$ with an accuracy of 1.2 arcsec (90 per cent confidence level). For additional information on the X-ray afterglow analysis see Margutti et al. (2013).

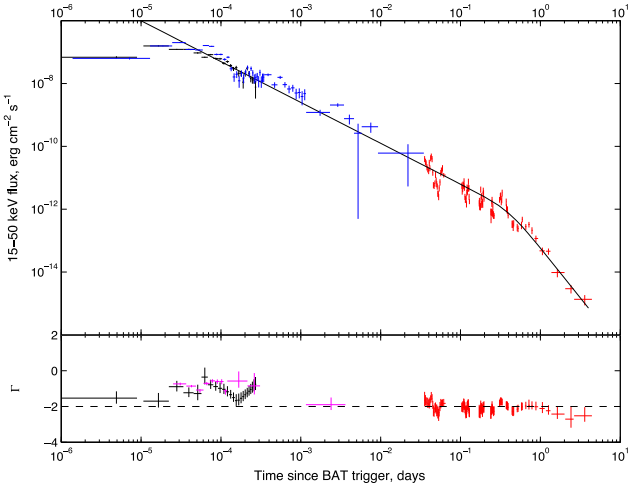

Figure 5. (top) The 15–50 keV X-ray light curve of GRB 051008 based on the data from the *Swift*/BAT (black crosses), *Swift*/XRT (red crosses), and *INTEGRAL*/SPI–ACS (blue crosses). The black solid line represents the best fit to the data using a broken PL (1); (bottom) photon indices Γ of the X-ray spectrum obtained by *Swift*/BAT (black crosses), *Swift*/XRT (red crosses), and Konus-*WIND* (magenta crosses).

Fig. 5 shows the flux light curve in the 15–50 keV energy range created using BAT, XRT,[6] and SPI-ACS data. The flux light curve can be created from a count rate light curve using a conversion factor computed from spectral and absorption models and instrumental response matrices. The procedure is not unreasonable if the photon index (Γ) varies smoothly with time (for more details see Evans et al. 2010). Indeed the photon index (Fig. 5, bottom panel) is seen to be monotonously decreasing from the end of the BAT data towards XRT via the Konus-*WIND* data in between.

Since the SPI-ACS experiment has no spectral channels we converted the SPI-ACS count rate light curve into a flux light curve in the energy range 15–50 keV in two steps. (1) Using the Konus-*WIND* CPL spectral model we calculated the fluence of the main activity episode (−25–98 s) in the 80 keV–10 MeV energy range (i.e. the SPI-ACS energy band), and we found a conversion coefficient (at the same time interval of the SPI-ACS) which is equal to $(2.5 \pm 0.7) \times 10^{-10}$ erg cm^{-2} per count. (2) Using the same CPL spectral model we converted the SPI-ACS fluence into the 15–50 keV energy range.

The resulting BAT+SPI-ACS+XRT flux light curve was fitted by a broken PL (see e.g. Beuermann et al. 1999):

$$F = F_0 \left[\left(\frac{t}{t_{\rm b}} \right)^{\alpha_1 w} + \left(\frac{t}{t_{\rm b}} \right)^{\alpha_2 w} \right]^{-1/w}, \quad (1)$$

where α_1 and α_2 are the initial and final flux decay indices; $t_{\rm b}$ is the time corresponding to the break in the light curve; w is the parameter responsible for the sharpness of the break, and F_0 is the normalization coefficient. Fig. 5 shows the light curve with the fit. The fit yields the following parameter values: $t_{\rm b} = 0.41 \pm 0.14$ d, $\alpha_1 = 1.30 \pm 0.18$, and $\alpha_2 = 3.18 \pm 0.20$. Among tested discrete values of break sharpness from 1 to 5 the best-fitted w equals 2.

The $t_b = 0.41 \pm 0.14$ d is somewhat larger than the one obtained in Racusin et al. (2009) ($t_b = 0.19 \pm 0.04$ d). It could be due to

[6] http://www.swift.ac.uk/burstanalyser/00158855/SHOWbatxrtlightcurves/TIMEDEL1/batxrtfluxwithgammaBATBANDBATTIMEDEL1.qdp.gz

different light-curve models being used, but primarily due to adding *Swift*/BAT and *INTERGRAL*/SPI-ACS data to the fit. Indeed, if we fit only the *Swift*/XRT data (Volnova et al. 2010a), we find this parameter to be in a good agreement with the results of Racusin et al. (2009). It is also evident that the afterglow light curve of GRB 051008 belongs to a less frequent class of plateau-less XRT light curves and may represent only phases III and IV of the canonical X-ray afterglow (Nousek et al. 2006; Zhang et al. 2006; Liang et al. 2009; Racusin et al. 2009).

2.5 Optical and NIR observations

The Crimean Astrophysical Observatory started observations of the burst error box with the 2.6-m Shajn telescope 32 min after the burst trigger (Rumyantsev, Biryukov & Pozanenko 2005). Close to the initial XRT error circle a source (Id1 in Fig. 6) was found, which however was later discarded as the OA of GRB 051008 (Pozanenko et al. 2007). The limiting R magnitude of the co-added frame with mean observing time 17:28:14 UT is 23.3 mag (see Tables 4 and 5).

The UVOT optical telescope of the *Swift* space observatory started to monitor the region of GRB 051008 at 17:23:49 UT, 50 min after the burst trigger (Roming, Marshall & Blustin 2005b). The telescope took a 200-s v-band image; no afterglow was found at a 5σ significance level for 18.2 mag (Breeveld, Marshall & Blustin 2005). The optical observations of the burst region were highly hindered by the presence of the bright $R \sim 5.5$ mag star HR 5096 2.5 arcmin from the XRT position.

Swift/UVOT continued observations of the GRB 051008 region up to Oct.14 using the ultraviolet filters u, $uvw1$, $uvm2$ and $uvw2$, with a total exposure of about 11 000 s in each filter, and the v filter with a total exposure of more than 120 000 s. Neither OT nor the host galaxy of the GRB was detected in stacked images in any UVOT filter, particularly up to $uvw2 > 23.2$.

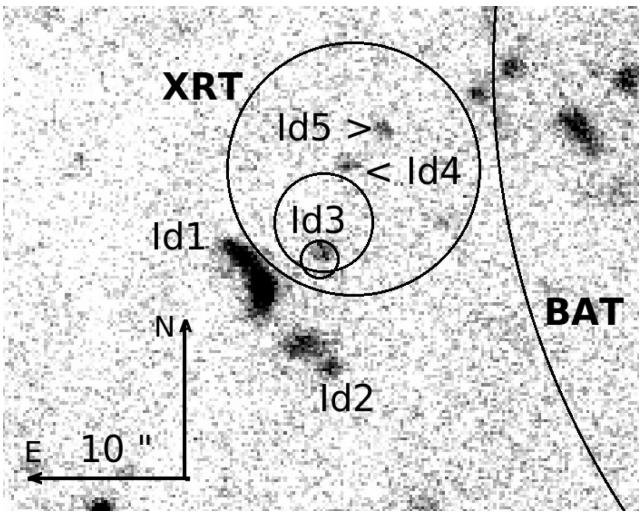

Figure 6. The localization of GRB 051008 and its immediate neighbourhood. The image was taken 255 d after the GRB in the R-band filter (the limiting magnitude is 25.7 mag) with a 4800 s exposure, using the NOT. The burst error circles determined from the *Swift*/BAT and the *Swift*/XRT telescopes data are shown with solid lines. An arc at the right side of the image is a part of BAT error circle. Three small circles denote different XRT error boxes. The position of the X-ray afterglow of the burst lies outside the refined BAT error circle. The smallest error box depicts the *Swift*/XRT refined error circle at (J2000) RA = $13^{\rm h}31^{\rm m}29\overset{\rm s}{.}55$, Dec. = $+42^\circ05'53\overset{''}{.}3$ with a radius of 1.2 arcsec (Butler 2007). The Id1-5 markers indicate the sources studied in this paper. The coordinates of the Id3 source are RA = $13^{\rm h}31^{\rm m}29\overset{\rm s}{.}510$, Dec. = $+42^\circ05'53\overset{''}{.}67$ (J2000) with an error of 0.08 arcsec in both right ascension and declination (statistical error only). The image scale and seeing are equal to 0.19 arcsec per pixel and 0.9 arcsec, respectively.

Observations of the field of GRB 051008 were obtained with the 1.34-m Schmidt telescope of the Thüringer Landessternwarte Tautenburg as soon as dusk fell, beginning 0.8 h after the GRB trigger (see Ferrero & Klose 2005; Ferrero et al. 2005; Klose & Hoegner 2005). Initial observations were obtained in the I_C band, lengthening the exposure times (2×10 s, 6×20 s, 7×120 s) in order to accommodate for the decrease in sky background. These observations were followed by sets of 6×120 s each in R_C and V. The halo of the bright nearby star influences the GRB position only in the R_C image, reducing the limiting magnitude.

We obtained further imaging with the TLS Schmidt ∼20 d after the GRB, around the expected peak-time of a low-z GRB supernova (Zeh, Klose & Hartmann 2004; Ferrero et al. 2005). We obtained 30×60 s exposures in the I_C band, and then $3 \times 30 \times 60$ s exposures in the R_C band in three consecutive nights. These observations were all obtained at high airmass (1.8–3.0). For the 90 min stacked R_C image, we carefully modelled and subtracted the flux of the nearby bright star. While strong residuals remain within 20 arcsec of the star's position, the GRB location is far enough away to have a smooth background. We clearly detect the galaxy Id1 and faintly detect the galaxy Id2 next to it. At the XRT position of the X-ray afterglow (and the host galaxy Id3 underneath it), no source is detected to $R_C > 22.7$. The I_C upper limit is significantly less deep and not constraining.

All TLS data were calibrated against two bright but non-saturated SDSS DR8 stars (stars 6 and 7 in Table 6), as the other stars were in most cases not even detected. SDSS AB magnitudes were transformed into Johnsons–Cousins Vega magnitudes analogue to the other calibration stars.

On 2006 April 28, a source candidate for the host galaxy of GRB 051008 was found as a result of observations made with the Shajn telescope of the Crimean Astrophysical Observatory (see Fig. 6, source Id3). The source was further observed in 2006–2009 with the Nordic Optical Telescope (NOT), the AZT-22 telescope of the Maidanak Observatory, and the Keck telescope. These observations allowed us to take images of the burst region in the $Bg'VRR_CI_C$ filters and in the interference filter i. In 2008 February and in 2012 February–March we obtained additional optical observations of the field using the Low Resolution Imaging Spectrometer (LRIS) on Keck. The series of frames were taken in the *UBIZ* filters with total exposure times of 930, 930, 810, and 720 s, respectively. All preliminary reductions were performed using private IDL codes. The best limiting magnitude was obtained in the filter $g' > 27.2$ mag, for the other limiting magnitudes see Table 4.

We acquired deep infrared imaging at the position of GRB 051008 using the Near-Infrared Imager (NIRI) on Gemini-North on the night of 2010 June 23, starting at 07:15 UT. 27 exposures of 60 s each were acquired on the field in the K' filter, which we reduced and stacked using the routines in the Gemini IRAF package. Unfortunately, there is only a single faint star (2MASS 13313142+4206470) in the FOV of the combined image, which a series of late-time PAIRITEL images suggests may be variable. Instead, since the night was photometric, we calibrate the host photometry using an observation of the IR standard star FS 29 taken later in the night of Gemini observations.

Table 4 presents the log of our observations of the GRB 051008 field. Fig. 6 displays the location of GRB 051008, indicating the supposed host galaxy, and the XRT and BAT error circles. Galaxies

Table 4. Log of optical and NIR observations of the GRB 051008 location. The magnitudes are not corrected for Galactic reddening.

Date	$t - t_0$ (d)	Telescope	Exposure, s	FWHM, (arcsec)	Filter	Upper limit, at the 3σ level
8.10.2005	0.034	TLS	20	1.3	I_C	16.0
8.10.2005	0.035	ZTSh	2200	2.1	R_C	23.3
8.10.2005	0.041	TLS	120	1.3	I_C	17.5
8.10.2005	0.049	TLS	840	1.4	I_C	19.3
8.10.2005	0.062	TLS	720	1.4	R_C	20.0
8.10.2005	0.074	TLS	720	1.6	V	21.5
8-10.10.2005	0.819	UVOT	11474	2.5	$uvw2$	23.2
8-10.10.2005	0.824	UVOT	10822	2.5	$uvw1$	22.5
8-10.10.2005	0.845	UVOT	11887	2.5	$uvm2$	22.7
8-10.10.2005	0.887	UVOT	11181	2.5	u	22.5
10-14.10.2005	4.128	UVOT	125336	2.5	v	22.8
27.10.2005	19.46	TLS	1800	1.7	I_C	20.0
29.10.2005	21.47	TLS	5400	2.5	R_C	22.7
28.04.2006	202.3	ZTSh	4260	1.9	R_C	24.1
20.06.2006	255.3	NOT	4800	0.9	R	25.7
30.06.2006	265.2	NOT	4800	1.2	V	25.7
25.07.2006	290.1	ZTSh	2760	1.5	R_C	23.5
12.08.2006	308.2	NOT	3300	0.7	B	25.9
20.08.2006	316.2	NOT	4200	0.9	i	22.5
16.09.2007	709.9	AZT-22	12120	2.0	I_C	22.5
12.02.2008	856.9	Keck I	780	0.85	R_C	26.1
12.02.2008	856.9	Keck I	960	0.85	g'	27.2
20.05.2009	1289.9	NOT	8400	1.1	i	23.9
24.06.2010	1719.0	Gemini	1620	0.5	K'	23.0
20.02.2012	2325.7	Keck I	930	1.8	B	25.8
20.02.2012	2325.7	Keck I	810	1.8	I	25.2
15.03.2012	2349.6	Keck I	930	1.1	U	25.4
15.03.2012	2349.6	Keck I	720	1.1	Z	25.5

Table 5. Photometric magnitudes (Vega) of the Id1-5 sources based on the observations made with the *Swift*/UVOT and TLS in 2005 October, ZTSh in 2006 April, the NOT in 2006 June–August and 2009 May, Keck in 2008–2012 and Gemini in 2010. The magnitudes displayed in the table are in the Vega photometric system and have been dereddened for Galactic extinction (Schlegel, Finkbeiner & Davis 1998). The photometry of the host galaxy is marked with bold type.

Filter	Id1 (mag)	Id2 (mag)	Id3 (**mag**)	Id4 (mag)	Id5 (mag)	Instrument
$uvw2$	21.69 (0.18)	22.29 (0.26)	>**23.3**	>23.3	>23.3	*Swift*/UVOT
$uvm2$	21.17 (0.16)	22.66 (0.33)	>**22.8**	>22.8	>22.8	*Swift*/UVOT
$uvw1$	21.31 (0.19)	22.30 (0.39)	>**22.6**	>22.6	>22.6	*Swift*/UVOT
u	21.32 (0.16)	>22.6	>**22.6**	>22.6	>22.6	*Swift*/UVOT
U	21.30 (0.04)	22.92 (0.07)	**25.32 (0.23)**	25.13 (0.19)	25.46 (0.28)	Keck I/LRIS
B	21.80 (0.20)	23.63 (0.21)	**25.20 (0.23)**	25.28 (0.27)	25.70 (0.26)	NOT/ALFOSC
B	22.12 (0.03)	23.44 (0.07)	**25.27 (0.13)**	25.22 (0.13)	25.67 (0.19)	Keck I/LRIS
g'	21.77 (0.05)	23.49 (0.07)	**24.57 (0.07)**	24.94 (0.13)	25.19 (0.19)	Keck I/LRIS
v	22.27 (0.29)	>22.8	>**22.8**	>22.8	>22.8	*Swift*/UVOT
V	21.50 (0.13)	22.93 (0.14)	**24.45 (0.13)**	24.75 (0.18)	24.91 (0.19)	NOT/ALFOSC
R	21.15 (0.04)	22.30 (0.09)	**24.07 (0.11)**	24.16 (0.12)	24.38 (0.11)	NOT/ALFOSC
R	21.35 (0.08)	22.42 (0.13)	**24.01 (0.24)**	>24.1	>24.1	ZTSh
R_C	21.22 (0.05)	22.39 (0.07)	**24.06 (0.10)**	24.13 (0.13)	24.33 (0.13)	Keck I/LRIS
R_C	21.18 (0.08)	22.28 (0.26)	>**22.7**	>22.7	>22.7	TLS
I	20.23 (0.03)	21.33 (0.02)	**23.88 (0.11)**	23.90 (0.11)	24.14 (0.14)	Keck I/LRIS
i	20.37 (0.05)	21.53 (0.06)	**24.01 (0.15)**	23.81 (0.17)	23.98 (0.16)	NOT/ALFOSC
Z	20.29 (0.08)	21.31 (0.09)	**23.80 (0.13)**	23.78 (0.18)	23.93 (0.18)	Keck I/LRIS
K'	18.49 (0.10)	19.18 (0.11)	**22.86 (0.29)**	>23.0	>23.0	Gemini/NIRI

Id1, Id2, Id4, and Id5 lie within a 10 arcsec radius circle around the probable host galaxy of GRB 051008 (Id3) and we will also study these galaxies below. Table 5 gives the results of the photometric reduction of the observations of this region.

All astrometric solutions were obtained using the APEX astrometric code (Devyatkin et al. 2010). All astrometric errors are statistical only if not stated otherwise. The reference catalogue for the astrometric reduction is USNO-B1.0. All photometric

Table 6. Reference stars used for the source photometry. The data are adopted from the SDSS-DR7 catalogue (Abazajian et al. 2009). The magnitudes are in the AB photometric system.

Star's ID	RA, J2000	Dec, J2000	*u*	*g*	*r*	*i*	*z*
J133138.56+420443.5	13 31 38.57	+42 04 43.6	22.110	20.507	20.028	19.826	19.755
J133137.89+420705.4	13 31 37.89	+42 07 05.5	20.073	19.010	18.831	18.742	18.694
J133141.93+420803.0	13 31 41.93	+42 08 03.1	23.900	22.618	21.203	19.684	18.925
J133146.39+420825.9	13 31 46.39	+42 08 25.9	21.217	19.594	19.097	18.827	18.755
J133145.90+420730.4	13 31 45.91	+42 07 30.4	22.789	20.456	19.836	19.586	19.367
J133133.58+420401.4	13 31 33.58	+42 04 01.5	15.456	13.973	13.497	13.769	13.286
J133153.54+420304.7	13 31 53.54	+42 03 04.8	19.365	16.792	15.435	14.779	14.414

calibrations for the data employed in this paper were performed using the method of relative aperture photometry via the APPHOT procedure of the IRAF software package[7] except for the *Swift*/UVOT data which were reduced using NASA's HEASARC software package HEASOFT.[8] The Id1 and Id2 sources have complex shapes and using the APPHOT procedure we therefore applied the apertures shaped as irregular closed polygons inscribed in the isophotes. For the photometric calibration of the $Bg'VRI$ images we used seven stars from the SDSS-DR7 catalogue (Abazajian et al. 2009) (see Table 6).[9] The transmission curves of the Keck *U* and *Z* filters do not match exactly the SDSS *u* and *z* bands. The *U* and *Z* images were calibrated using the relative magnitude averaged by 14 non-overexposed stars of the field. The stars were chosen with the aid of an on-line software package which we use to search for secondary photometric standards in the FOV of GRBs from automatic GCN notices (BACODINEs) Pozanenko et al. (in preparation). To process *Swift*/UVOT data we used the task UVOTIMSUM of the HEASOFT package to combine all frames for each filter (*u*, *uvw*1, *uvm*2, *uvw*2 and *v*) and the task UVOTSOURCE to obtain the magnitudes of the sources Id1–5. The calibration and upper limit estimates were done using the HEASARC CALibration Data Base (CALDB[10]). For the galaxies Id3–5 we used circular apertures with a fixed radius of 2.2 arcsec. For the Id1 and Id2 galaxies we increased this radius to 5.0 arcsec.

2.6 Spectroscopy of the host galaxy

We obtained a longslit spectrum of the host galaxy of GRB 051008 on the night of 2009 June 25 (UT) using the LRIS (Oke et al. 1995) on the Keck I 10-m telescope. Three exposures of 900 s each were acquired on the source at a position angle of 202°, using the D560 dichroic, 600-line grism (blue), and 400-line grating (red). The target was acquired independently before each of the three 900 s exposures and no additional dithering was performed, so the exposures are effectively undithered aside from small differences of less than 1 arcsec. No obvious line features are identified in the sky-subtracted 2D spectra.

2.7 Radio observations

GRB 051008 was observed by the Very Large Array. No radio afterglow was detected. An 8.5 GHz flux upper limit of 0.12 mJy was obtained for the burst location region on 2005 Oct. 8, at 20:30:24 UT, i.e. four hours after the trigger (Cameron 2005, see also Chandra & Frail 2012). Further observations carried out 2 d after the trigger on Oct. 10, 18:57:36 UT at the same frequency obtained a flux upper limit of 0.11 mJy.[11]

The position was also re-observed on 2012 June, 11 with the upgraded Karl G. Jansky Very Large Array as part of the host-galaxy study of Perley & Perley (2013). No source was detected consistent with the XRT position with a 2σ upper limit of 0.014 mJy at 5.23 GHz.

3 PROPERTIES OF THE HOST GALAXY

The coordinates of the Id3 source (Fig. 6) are RA = $13^{h}31^{m}29^{s}.510$, Dec. = $+42°05'53''.67$ (J2000), accurate to within 0.08 arcsec in both coordinates (statistical error). The source lies inside the final XRT 1.2 arcsec-error box corrected using the joint observations of the source field performed by the XRT and the centroids of corresponding optical sources in the SDSS-DR5 catalogue (Butler 2007). However, this match may be accidental. Bloom, Kulkarni & Djorgovski (2002) reported a formula for computing the probability of finding a galaxy inside an arbitrary sky area as a function of the galaxy magnitude. For GRB 051008 it yields a probability of about 1.96 per cent for an accidental location of the Id3 galaxy inside the XRT error circle.

In a circle with centre at Id3 and radius of 10 arcsec there are five galaxies. One can assume that these galaxies compose a group. We will investigate it below.

We used the LE PHARE software package (Arnouts et al. 1999; Ilbert et al. 2006) to estimate the redshifts of the galaxies Id1–5 from the photometric data obtained with the NOT, Keck I, and Gemini North. We found a photometric redshift of $z = 2.77^{+0.15}_{-0.20}$ (95 per cent confidence level) for the host galaxy. An independent analysis of the redshift based only on the Keck observations shows $z = 2.90^{+0.29}_{-0.16}$ at the same confidence level (Perley et al. 2013). Table 7 lists the estimated redshift values and other parameters of the galaxies Id1-5 including those determined using LE PHARE: the most probable galaxy SED type, the best-fitted extinction law, internal bulk extinction in the galaxy, and age of the dominant stellar population of the galaxy. We used the PEGASE2 population synthesis models library (Fiok & Rocca-Volmerange 1997) to obtain the best-fitted SED, the redshift, and the other required parameters. For all five galaxies we tried three different reddening laws: LMC (Fitzpatrick 1986), SMC (Prévot et al. 1984), and the reddening law for starburst galaxies (Calzetti et al. 2000). In case of the galaxy Id3 the best fit is the LMC reddening law. The best-fitting reddening laws for the galaxies Id1,2,4,5 are listed in Table 7. Fig. 7(a) shows

[7] http://iraf.noao.edu/
[8] http://heasarc.nasa.gov/docs/software/lheasoft/
[9] Magnitudes are converted from the *ugriz* into the *BVRI* system using Lupton's transformations http://www.sdss.org/dr7/algorithms/sdssUBVRITransform.html
[10] http://heasarc.gsfc.nasa.gov/FTP/caldb
[11] http://www.aoc.nrao.edu/~dfrail/grb051008.dat

Table 7. Parameters of the Id1-5 galaxies determined using Le Phare. Column 1 gives the galaxy ID; Column 2 – the photometric redshift with 95 per cent confidence level errors; Column 3 – the corresponding probability; Column 4 – corresponding χ^2 per degree of freedom; Column 5 – the most likely galaxy SED type (Im – irregular and interacting galaxies; B – starburst galaxies); Column 6 – the best fitted reddening law (LMC – the law for Large Magellanic Cloud; Fitzpatrick 1986, SMC – the law for Small Magellanic Cloud; Prévot et al. 1984, sb – the law for starburst galaxies; Calzetti et al. 2000), Column 7 – the age of the dominant stellar population of the galaxy in Gyr; Column 8 – the internal extinction in the galaxy; Column 9 – the *R*-band absolute magnitude of the galaxy, and Column 10 gives the size of the galaxy in kpc.

Id	$z \pm \Delta z$	Probability (per cent)	χ^2/DOF	Type of SED	Ext.law	Age (Gyr)	A_V (mag)	M_R (mag)	d (kpc)
1	$0.73^{+0.10}_{-0.08}$	>99.99	46/13	Im	sb	0.50	0.28	−22.26	49.7 ± 1.4
2	$0.70^{+0.11}_{-0.08}$	>99.99	54/13	Im	sb	0.60	0.35	−21.23	46.3 ± 2.6
3	$\mathbf{2.77^{+0.15}_{-0.20}}$	**96.32**	4.0/9	**B**	LMC	**0.06**	**0.31**	**−22.79**	**<7.2**
4	$2.76^{+0.14}_{-0.12}$	99.98	4.8/9	B	sb	0.02	0.49	−21.60	<7.2
5	$2.84^{+0.16}_{-0.19}$	98.23	5.0/9	B	LMC	0.05	0.03	−22.30	<7.2

the best-fitting SED of the galaxy Id3. It reveals that the burst occurred in a moderately absorbed LBG. It is one of the few cases where a LBG hosts a GRB (see also Odewahn et al. 1998; Jakobsson et al. 2005a; Malesani et al. 2013).

The redshift of $z = 2.77$ corresponds to a luminosity distance of 23.5 Gpc and a distance modulus of 46.8 mag, one arcsec corresponds to 8.0 proper kpc. For the galaxies Id3–Id5 the angular size is estimated as the full width at half-maximum of the point spread function during the observations made on 2008 February 12 (see Table 7), which is equal to 0.9 arcsec.

It is worth noting that the galaxies Id1 and Id2 have redshifts of $z_{\rm Id1} = 0.73^{+0.10}_{-0.08}$ and $z_{\rm Id2} = 0.70^{+0.11}_{-0.08}$ (95 per cent confidence level) with corresponding probability of >99.99 per cent. These redshifts differ from those of the three other galaxies. This is a foreground group of at least two irregular interacting galaxies situated at a redshift of $z \sim 0.7$. SEDs of all studied galaxies except for Id3 are shown in Fig. 7(b).

Evans et al. (2009) used the spectrum of the GRB X-ray afterglow to determine the hydrogen column density along the line of sight in the host galaxy of GRB 051008: $N_{\rm H} = (3.15 \pm 0.35) \times 10^{21}$ cm^{-2} (the provided redshift of the absorber is equal to 0). We used the $N_{\rm H}$–redshift-limit relation from Grupe et al. (2007) to estimate the upper limit of the GRB 051008 redshift to be $z < 2.8$. While the upper limit is consistent with our photo-z estimate one can note that this method is based on a sample of unobscured bursts, and may be biased towards lower upper limits. It is known that for optically dark bursts $N_{\rm H}$ values tend to be systematically higher (e.g. Fynbo et al. 2009; Krühler et al. 2012a; see also Table 10).

We estimate the SFR in the galaxy from its ultraviolet luminosity according to Kennicut (1998). Using the best-fitted SED and the best host extinction law one can estimate the UV luminosity of Id3 to be $L_{\rm UV} \sim 4.5 \times 10^{29}$ erg s^{-1} Hz^{-1}. For the SFR it gives an estimate of $\sim$60 M$_\odot$ yr^{-1}. The Le Phare package with the PEGASE2 library also gives the best-fitted values of the host physical parameters: star formation rate SFR$_{\rm PEGASE2} \sim 60$ M$_\odot$ yr^{-1} and the stellar mass of the galaxy $M \sim 1.2 \times 10^9$ M$_\odot$.

In comparison with LBGs with L^* luminosity Id3 is slightly under-luminous (by $\sim$0.5 mag in the rest-frame V band) and has bluer colours. The age of the dominant stellar population of 60 Myr is five times less than the average value for LBGs, which is not unusual for LBGs: about 25 per cent of LBGs have age <40 Myr

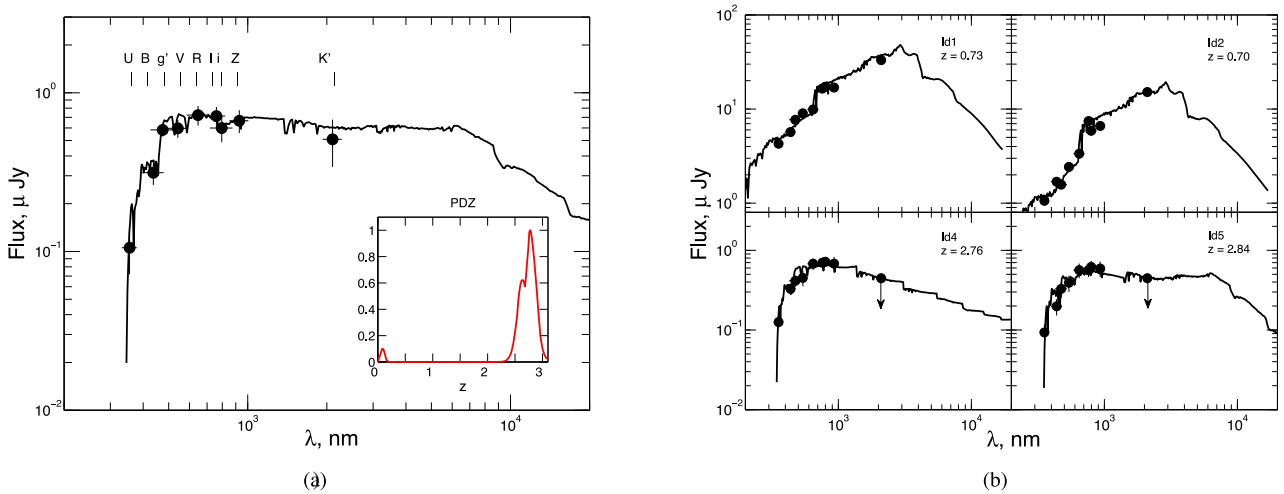

Figure 7. (a) Spectral energy distribution (SED) of the galaxy Id3 in the observer frame. The best-fitted SED type obtained by Le Phare (line) is the SED of a starburst galaxy. Observed flux in *UBg′VRiIZK′* filters is shown by black circles. The associated Probability Distribution Function is shown in the inset. (b) The best-fitted SEDs of the galaxies Id1, Id2, Id4 and Id5 obtained by Le Phare with observational data marked as in (a).

(Shapely et al. 2001). Also the Id3 galaxy is less dusty than an average LBG and 10 times less massive. Its SFR is less than the average LBG SFR, but close to it.

4 PROPERTIES OF GRB 051008 AND ITS AFTERGLOW

The X-ray afterglow data from *Swift*/XRT [12] provide the 2–10 keV flux for the time interval from 3070 to 445 845 s after the burst onset. 11 hours after the burst the X-ray flux was equal to 1.083×10^{-12} erg cm^{-2} s^{-1}. The 3-keV spectral density of the X-ray flux at 11 h after the trigger, converted in accordance with Jakobsson et al. (2004), is $F_{\rm X}(3\ {\rm keV}, 11^{\rm h}) = 0.018 \times 10^{-6}$ Jy. Assuming that the break at ∼0.41 d (see Section 2.4) is the achromatic jet-break we extrapolated the optical upper limit of 23.3 mag towards 11 h after the trigger using the XRT light curve. We estimate the optical flux to be $F_{\rm O}(R, 11^{\rm h}) < 0.068 \times 10^{-6}$ Jy. From this we derive $\beta_{\rm OX}(11^{\rm h}) \leq 0.02$, which allows us to classify this event as a dark burst. Since the spectral slope in X-ray regime is $\beta_{\rm X} = 1.1$ (see the end of this section), this burst is also dark according to the van der Horst et al. (2009) criterion.

We calculated the limit of the isotropic-equivalent radiated energy, using the redshift value, as $E_{\rm iso} = (1.13 \pm 0.20) \times 10^{54}$ erg (in the energy range 20 keV–10 MeV), and it is a lower estimate based on Konus-*WIND* measurements (see Section 2.2). Performing *k*-correction (e.g. Bloom, Frail & Sari 2001) $E_{\rm iso,\,corrected} = (1.15 \pm 0.20) \times 10^{54}$ erg. The collimated energy can be estimated given $E_{\rm iso}$ and the opening angle of the jet. To calculate the jet opening angle of GRB 051008, we use the corresponding formula from Sari, Piran & Halpern (1999) and Liang et al. (2007), which relates this parameter to the isotropic-equivalent radiated energy $E_{\rm iso}$ and the break time $t_{\rm b} = 0.41$ d of the afterglow light curve (see Section 2.4):

$$\theta_{\rm j} \sim 0.161 \left(\frac{t_{\rm b}}{1+z}\right)^{3/8} \left(\frac{E_{\rm K,iso,52}}{n}\right)^{-1/8}. \quad (2)$$

Here n is the constant ISM density, and $E_{\rm K,\,iso,\,52}$ is the total isotropic kinetic energy of the outburst in the units of 10^{52} erg. The latter value is related to the isotropic-equivalent energy via a formula $E_{\rm iso} = \xi E_{\rm K,\,iso}$, where ξ is the coefficient of conversion of the kinetic energy of the outburst into radiation energy, which depends on the ambient medium of the GRB source. We assume that the density of the medium and the conversion coefficient are equal to $n = 1$ and $\xi = 0.1$ (e.g. Zhang et al. 2007), respectively. Given the redshift, the break time of the light curve, and the equivalent isotropic energy, we estimate the jet opening angle as $\theta_{\rm j,\,ISM} = 1\overset{\circ}{.}7 \pm 0\overset{\circ}{.}2$. Taking these values into account, the collimation-corrected gamma-ray energy can be estimated as $E_{\gamma,\,\rm ISM} = (4.80 \pm 1.52) \times 10^{50}$ erg.

If the GRB progenitor is situated in a wind environment one can use equation (5) from Chevalier & Li (2000) which connects the jet opening angle θ and the parameters of the wind-like medium:

$$\gamma = 5.9 \left(\frac{1+z}{2}\right)^{1/4} E_{52}^{1/4} A_*^{-1/4} t_{\rm b,days}^{-1/4}, \theta_{\rm j} = 1/\gamma, \quad (3)$$

where E_{52} is the isotropic-equivalent energy in units of 10^{52} erg, $t_{\rm b,\,days}$ is the jet-break time in days, and A_* is a parameter of the medium, related to the density profile as following: $n = Ar^{-2}$, and $A = A_* \times 5 \times 10^{35}$ cm^{-1}. Assuming $A_* = 1$ we can estimate the value

[12] http://www.swift.ac.uk/xrt∼curves/00158855/flux.qdp

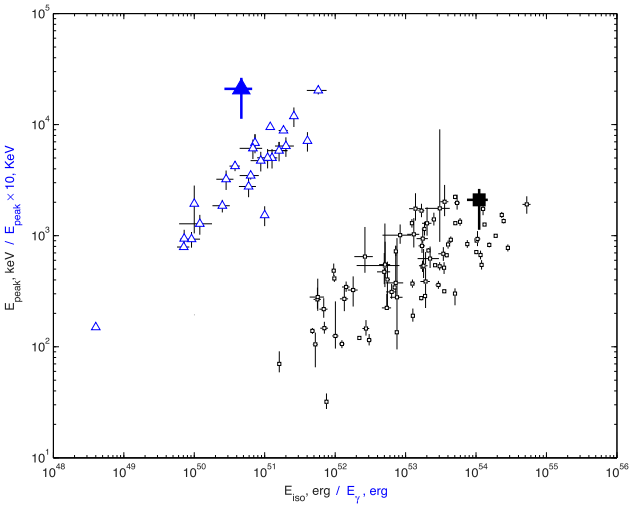

Figure 8. The Amati (squares; Amati 2006) and the Ghirlanda (triangles; Ghirlanda, Ghisellini & Lazzati 2004) diagrams. The Amati diagram displays the dependence of the energy corresponding to the maximum in the spectrum, $E_p(1+z)$, on the isotropic equivalent energy, $E_{\rm iso}$. The Ghirlanda diagram displays the dependence of the energy $E_p(1+z)$ on the collimated energy, E_γ (adapted from Ghirlanda et al. 2004). Filled symbols indicate the data points corresponding to GRB 051008, which can be seen to be in agreement with the Amati relation, but is a moderately significant outlier of the Ghirlanda relation assuming $z = 2.77$. The Ghirlanda diagram is shifted up along the *Y*-axis by a factor of 10 for clarity.

of the jet opening angle $\theta_{\rm j,\,wind} = 2\overset{\circ}{.}0 \pm 0\overset{\circ}{.}2$ and corresponding collimated gamma radiation energy $E_{\gamma,\,\rm wind} = (7.20 \pm 1.54) \times 10^{50}$ erg.

Using the value of the peak energy in the burst spectrum, we can plot the parameters of GRB 051008 in the Amati diagram (Amati 2006). Data of 95 GRBs used for the Amati diagram (Fig. 8) were taken from Konus-*WIND* observations. Additionally, using θ_j one can put GRB 051008 in the Ghirlanda diagram (Ghirlanda et al. 2004), an empirical diagram showing the correlation between the peak energy in the spectrum and the emitted γ-ray energy, i.e. $E_{\rm iso}$ corrected for the jet collimation (see Fig. 8). While the GRB fits well into the Amati correlation, it is evident that in case of an ISM environment, it does not agree with the Ghirlanda correlation. For the possible explanation see Section 5.1.

We extracted the X-ray spectrum from the raw *Swift*/XRT data using the XSPEC V12 software (a part of the HEASOFT software package[13]) for two different epochs: (a) $t - t_0 = 3072$–5393 s (∼50 min after the trigger) and (b) $t - T_0 = 14806$–17031 s (i.e. ∼4 h after the trigger). The data were calibrated using the HEASARC CALibration Data Base (CALDB[14]) and fitted with single PL with two absorption models (*phabs*zphabs*powerlaw*). The values of the Galactic absorption of $N_{\rm H,\,Gal} = 1.05 \times 10^{20}$ cm^{-2} and the redshift of $z = 2.77$ were fixed. The fitting provided the value of the host absorption at the assumed redshift of $N_{\rm H,\,host}(a) = (7.7 \pm 1.2) \times 10^{22}$ cm^{-2}, $N_{\rm H,\,host}(b) = (7.9 \pm 1.6) \times 10^{22}$ cm^{-2} and the photon index $\Gamma(a) = 1.8 \pm 0.1$, $\Gamma(b) = 2.1 \pm 0.2$. The value of $N_{\rm H,\,host}$ is one of the highest known, even for dark bursts (see Table 10). Using these data we can estimate the extinction along the line of sight to the GRB source. We construct the optical SED of the afterglow

[13] http://heasarc.gsfc.nasa.gov/docs/software/lheasoft/
[14] http://heasarc.gsfc.nasa.gov/FTP/caldb

extrapolating the XRT spectral slope to the optical bandwidth with a cooling break in the soft end of the X-ray spectrum (the most conservative estimation). Next, we apply the LMC extinction law in the host galaxy to the model of the SED (see Section 3). Then we normalize the model of the optical SED to the upper limit obtained in the same epoch using the early Shajn observation. The resulting value of the total extinction $A_V^{\rm total}$ in the rest frame is 3 mag (which effectively is a lower limit for the total extinction). The intrinsic extinction in the host galaxy is $A_V^{\rm host} = 0.31$ mag. This value may vary significantly depending on the specific sightline through the galaxy even if we assume a homogeneous distribution of the absorbing interstellar medium. For a conservative estimation we assume $A_V^{\rm host} \sim 1$ mag. Thus the source suffers from additional extinction along the line of sight $A_V^{\rm LOS} > 2$ mag. This indicates that there is an additional absorber in the line of site.

5 DISCUSSION

5.1 Properties of GRB 051008

The summary of the properties of GRB 051008 and its host galaxy are listed in Tables 8 and 9. We would like to emphasize several properties of GRB 051008. The absence of statistically significant spectral lag places the burst in the top 17 per cent of the Konus-*WIND* burst sample and into the ∼10 per cent of long bursts without spectral lag in the BATSE (Hakkila et al. 2007) and *Swift* (Ukwatta et al. 2010) samples. The hardness of the burst, especially the high $E_{\rm peak} = 770$ (CPL) keV of the main peak of the GRB, which corresponds to ≈2.9 MeV in the rest frame and places the burst in the 7 per cent of hardest time-resolved spectra of the BATSE sample (Kaneko et al. 2006).

GRB 051008 is clearly a long duration burst ($T_{90} = 214$ s as seen by Konus-*WIND* and $T_{90} = 535$ s as seen by SPI-ACS). The burst consists of a hard main peak and a somewhat softer tail detectable up to ∼800 s. As we have seen from the joint BAT, SPI-ACS and XRT analysis the light curve can be described by a single PL after the main peak of the burst up to the jet-break episode. The burst belongs to the less-frequent class of plateau-less X-ray afterglows (Liang et al. 2009).

From the modelling of the SED of the host galaxy one can conclude that GRB 051008 is optically dark neither because of high redshift ($z = 2.77$), nor due to the global absorption in the host galaxy $A_V = 0.31$ mag. The lack of an OA is likely caused by absorption in the circumburst medium or by a dense cloud along the line of sight.

The burst is an outlier of the Ghirlanda relation assuming a value for the ISM density, $n = 1$. An option to make GRB 051008 agree with the Ghirlanda diagram is that the density of the ISM could be drastically higher, $n = 10^4 - 10^6$ instead of $n = 1$ used in our previous estimates. In case of a wind profile, we can estimate the necessary normalization in the density profile A of $n = Ar^{-2}$ needed to fulfil the Ghirlanda relation. Let us assume $E_\gamma = 8.2 \times 10^{51}$ erg which would be needed to put GRB 051008 on the Ghirlanda relation. This yields the value of the jet opening angle to be $\theta \approx 7^\circ$. Using equation (5) from Chevalier & Li (2000) we obtain the value of $A_* = 140\,{\rm cm}^{-1}$, and $A = A_* \times 5 \times 10^{35}\,{\rm cm}^{-1} = 4.2 \times 10^{37}\,{\rm cm}^{-1}$. The normalization is ∼100 times greater than the typical wind parameters of Wolf–Rayet stars (e.g. Castro-Tirado et al. 2010). This fact supports the hypothesis that the burst progenitor is embedded in a dense circumburst medium with a density of $n = 10^4 - 10^6\,{\rm cm}^{-3}$ rather than the absorber being along the line of sight.

If we suggest a high density of a circumburst medium, one might expect an appearance of a bright radio counterpart. For example, for GRB 111215A (Zauderer et al. 2013) the maximum of the radio afterglow light curve at 5.8 GHz was observed approximately 15 d after the burst at the level of about 1 mJy. Unfortunately, there were no long-term radio observations of GRB 051008 and deep upper limits (see Section 2.6) are not in contradiction with a possible radio afterglow evolution similar to that obtained for GRB 111215A by Zauderer et al. (2013).

Finally, the fact that the redshifts of two further galaxies (Ids 4, 5, Table 7) are close to $z_{\rm Id3} = 2.77^{+0.15}_{-0.20}$ may support the hypothesis that the host galaxy could be gravitationally paired with at least one other galaxy at a projected distance of about 50 kpc. The distance between the galaxies Id3 and Id4 is 46 ± 10 kpc, if we adopt a common redshift of $z = 2.77$.

Table 8. Summary of the properties of the host.

RA	$13^{\rm h}31^{\rm m}29\overset{\rm s}{.}510$
Dec.	$+42^\circ05'53\overset{''}{.}67$
$z_{\rm phot}$	2.77 (+0.15, −0.20) (95 per cent confidence level)
SED type	Starburst
$A_{V,\rm bulk}$	∼0.31 mag
M_B	−21.6 ± 0.3 mag
M_R	−22.8 ± 0.1 mag
$M_{K'}$	−23.9 ± 0.3 mag
Age	60 Myr
Mass	$1.2 \times 10^9\,{\rm M}_\odot$
SFR	$\sim 60\,{\rm M}_\odot/{\rm y}$

Table 9. Summary of the GRB and afterglow properties.

$N_{\rm H,\,z}$	$(7.9 \pm 1.6) \times 10^{22}\,{\rm cm}^{-2}$	
$E_{\rm iso}$	$(1.15 \pm 0.20) \times 10^{54}$ erg	
$t_{\rm b}$	0.41 ± 0.14 d	
α_1	1.30 ± 0.18	
α_2	3.18 ± 0.20	
$\beta_{\rm OX}$ (11 h)	<0.02	
$\beta_{\rm X}$ (4 h)	1.1 ± 0.2	
	ISM	Wind
θ_j	$1\overset{\circ}{.}7 \pm 0\overset{\circ}{.}2$	$2\overset{\circ}{.}0 \pm 0\overset{\circ}{.}2$
E_γ	$(4.80 \pm 1.52) \times 10^{50}$ erg	$(7.20 \pm 1.54) \times 10^{50}$ erg.

5.2 Comparison with other dark bursts

Table 10 lists the parameters of dark bursts for which host galaxies have been found. The table partially overlaps with the dark burst sample presented by Perley et al. (2013). Our table lists the following parameters of the galaxies: redshift, apparent and absolute *R*-band magnitudes, colour information, intrinsic host absorption, absorption along the line of sight to the GRB source, hydrogen column density, and SFR. It comes as no surprise that the GRBs presented in Table 10 exhibit high line-of-sight extinction, since the assumption employed in selecting this sample (i.e. a redshift that does not point to the influence of Lyman absorption, and the application of a single synchrotron spectrum in modelling the broad-band SED) leaves extinction as the strongest choice to explain the optical/NIR darkness (Krühler et al. 2012a; Perley et al. 2013). We also find that many dark-burst host galaxies exhibit a high SFR, with the median SFR for $z > 1$ hosts in our list being ≈40 $\rm M_\odot\ yr^{-1}$. Indeed, GRB 051008 is one of the most distant bursts for which a host galaxy has been investigated in detail.

Table 10. A comparison of the parameters of host galaxies of dark GRBs. Column 1 lists the name of the burst associated with the galaxy; Columns 2–4 indicate whether the burst had any X-ray, optical/NIR, or radio afterglow ('IR' means the detection of the OA only in the infrared domain, 'n' means that no observations were made in the wavelength interval considered); Column 5 gives the spectral index (^{x} – the spectral index $\beta_X - 0.5$ is adopted according to the van der Horst et al. 2009 darkness criterion); Column 6 lists the redshift (superscript ^{p} indicates that the redshift was determined photometrically); Column 7 gives the *R* magnitude of the host galaxy; Column 8 presents the data on the colour of the galaxy; Column 9 gives internal bulk extinction in the galaxy; Column 10 – the extinction towards the GRB source along the line of sight; Column 11 – the hydrogen column density; Column 12 – the absolute *R*-band magnitude of the galaxy; Column 13 – the SFR, and Column 14 – references: 1 – Djorgovski et al. (2001), 2 – Bloom et al. (2003), 3 – Gorosabel et al. (2003), 4 – Piro et al. (2002), 5 – Frail et al. (2003), 6 – Jakobsson et al. (2005b), 7 – Küpcü Yoldaş et al. (2010), 8 – Levan et al. (2006), 9 – Perley et al. (2013), 10 – Castro-Tirado et al. (2007), 11 – Perley et al. (2009), 12 – Tanvir et al. (2008), 13 – Jaunsen et al. (2008), 14 – Elíasdóttir et al. (2009), 15 – Svensson et al. (2012), 16 – Krühler et al. (2012a), 17 – Hunt et al. (2011), 18 – Hashimoto et al. (2010), 19 – Krühler et al. (2011), 20 – Krühler et al. (2012b), 21 – Chen et al. (2010), 22 – Holland et al. (2010), 23 – Greiner et al. (2013), * refers to the present paper.

GRB	*X*	*O*	*R*	β_{OX}	*z*	R_{host} (mag)	Colour (mag)	$A_{V,host}$ (mag)	$A_{V,LOS}$ (mag)	$N_H \times 10^{21}$, (cm^{-2})	M_R, ^{m} (mag)	SFR, ($M_\odot$ yr^{-1})	Reference
970828	+	−	+	0.09	0.96	25.2	$R-K=3.7$	—	>3.8	>6	−19.6	∼1.2	(1)
990506	+	−	+	<0.06	1.31	24.3	$(R-K)_{AB}=2.3$	>1	—	—	−20.5	12.6	(2)
000210	+	−	+	0.44	0.85	25.0	$R-K=2.5$	∼0	—	5 ± 1	−22.2	∼2.1	(3,4,5)
							$V-I\sim1.7$						
020819	n	−	+	—	0.41	23.46	$R-K=2.7$	1.8−2.6	4−20	—	−22.3	<40	(6,7)
030115	+	+	+	—	$2.5-2.7^p$	25.58^a	$R-K=5.35$	∼1.0	—	—	—	$4.4-500$	(8)
050915A	+	−	n	0.23	2.53	24.56	$R-K=3.9$	1.0	∼1.4	$0.9^{+0.8}_{-0.7}$	−22.1	$135.8^{+63.1}_{-48.3}$	(9)
051008	+	−	−	<0.02	2.77^p	24.06	$V-I=0.6$	0.31	>2	79 ± 16	−22.8	∼60	(*)
							$R-K=1.4$						
051022	+	−	+	<−0.11	0.81	21.5	$R-K=3.3$	1.0	>9	$34.7^{+4.8}_{-4.7}$	−21.8	∼50	(9,10)
							$V-I\sim1.1$						
060202	+	−	n	<0.20	0.78	23.79^b	$(R-K)_{AB}=1.1$	∼1	2.9	$4.5^{+0.7}_{-0.6}$	−19.6	$5.8^{+1.3}_{-1.9}$	(9)
060210	+	+	−	0.37	3.91	24.33^b	$(R-I)_{AB}\approx0.1$	0.25	$1.2^{+0.2}_{-0.1}$	$24.6^{+2.9}_{-3.5}$	<−20.2	−23.4	(11)
060306	+	−	n	<0.21	1.55	24.49^b	$(R-K)_{AB}=2.5$	2.2 ± 0.1	4.6	$3.0^{+0.8}_{-0.7}$	−20.8	244^{+129}_{-67}	(9)
060319	+	+	n	0.19	1.17	24.20^b	$(R-K)_{AB}=2.4$	$0.1^{+0.2}_{-0.1}$	1.1	$3.4^{+0.8}_{-0.7}$	−20.3	$0.0^{+0.4}_{-0.0}$	(9)
060719	+	+	−	−0.27	1.53	24.62^b	$(R-K)_{AB}=1.8$	$0.4^{+1.1}_{-0.4}$	2.1	$3.4^{+1.3}_{-1.0}$	−20.6	$4.0^{+36.9}_{-4.0}$	(9)
060814	+	+	n	−0.21	1.92	22.85	$(R-K)_{AB}=1.2$	$1.2^{+0.1}_{-0.0}$	3.1	$2.7^{+0.4}_{-0.3}$	−23.0	$236.7^{+28.4}_{-18.3}$	(9)
060923A	+	+	−	0.38	$<2.8^p$	25.65	$R-K\sim4$	—	2.6	—	<−21.2	—	(11,12)
							$V-I\sim1.5$						
061222A	+	$+^{IR}$	+	<−0.19	2.09	24.93	$(V-I)_{AB}\sim0.5$	<0.5	>5.0	$44.8^{+5.4}_{-3.0}$	−21.2	—	(9,11)
							$(I-K)_{AB}<1.0$						
070306	+	$+^{IR}$	−	0.33	1.50	∼23	$R-K\sim1.5$	≤0.45	5.5 ± 0.6	$26.8^{+4.7}_{-4.3}$	−22.2	∼7.3	(13)
070521	+	−	n	<−0.10	1.35	26.11	$V-I=0.72$	—	>9	54^{+13}_{-11}	−18.8	—	(11)
070802	+	+	n	0.46	2.45	25.03	$R-K\sim3.3$	<1.5	<0.3	3.2 ± 1.8	−21.0	—	(14)
071021	+	$+^{IR}$	+	0.37	2.45	25.22^b	$(R-K)_{AB}=3.1$	1.6 ± 0.3	0.5	$0.5^{+0.8}_{-0.5}$	−21.3	108^{+98}_{-55}	(9)
080207	+	−	n	<0.3	2.08	>25.65	$R-K>5.4$	∼1.9	≤3.4	151^{+23}_{-22}	>−19.9	∼40	(15,16)
					$\sim2.2^p$	∼25.8	$R-K\sim6.3$	1 − 2	—			∼119	(17)
080325	+	$+^{IR}$	n	0.14 − 0.33	1.78	25.5	$R-K_s=3.8$	0.8	2.7 − 10	18^{+8}_{-6}	−20.3	10 − 80	(18,9)
080605	+	+	n	0.17^x	1.64	21.6	$(R-K)_{AB}=0.5$	0.5 ± 0.1	1.2 ± 0.1	9.0 ± 0.9	−22.4	49^{+26}_{-13}	(19,20)
080607	+	+	n	0.14 − 0.37	3.04	26.33^b	$(R-K)_{AB}=2.5$	1.25	3.3	1.4 ± 0.4	−20.8	$18.3^{+5.0}_{-3.2}$	(9,21)
081109A	+	+	−	<0.44	0.97	22.65	$(R-K)_{AB}=1.6$	1.0 ± 0.2	$3.4^{+0.4}_{-0.3}$	9 ± 2	−21.4	33^{+19}_{-13}	(19)
081221	+	+	+	0.00	2.26	24.67^b	$(R-K)_{AB}=2.5$	1.4 ± 0.1	1.4	$3.9^{+0.5}_{-0.4}$	−21.6	73^{+16}_{-13}	(9)
090404	+	−	+	<0.20	3.0^p	26.07^b	$(R-K)_{AB}=3.1$	$1.3^{+2.2}_{-1.2}$	1.3	$5.1^{+1.0}_{-0.9}$	−21.0	40^{+178}_{-22}	(9)
090407	+	−	n	<0.14	1.45	25.78^b	$(R-K)_{AB}=3.3$	$1.8^{+0.1}_{-1.2}$	1.6	2.3 ± 0.4	−19.3	$16.6^{+1.8}_{-15.2}$	(9)
090417B	+	−	−	<0.28	0.34	21.34	$R-K=2.8$	0.9 ± 0.1	2.7	$8.3^{+1.4}_{-1.2}$	−20.0	0.5 ± 0.3	(9,22)
090709A	+	−	−	−0.56	1.8^p	26.39^b	$(R-K)_{AB}=2.7$	$1.4^{+0.1}_{-0.2}$	3.0	1.7 ± 0.3	−19.3	$8.3^{+4.4}_{-3.6}$	(9)
090926B	+	+	n	0.23^x	1.24	22.94	$(R-K)_{AB}=1.5$	1.4 ± 0.3	$1.4^{+1.1}_{-0.6}$	$13.9^{+1.6}_{-1.5}$	−21.8	80^{+110}_{-50}	(19)
100621A	+	+	n	0.39	0.542	21.53	$(R-K)_{AB}=0.3$	0.6 ± 0.1	3.8 ± 0.2	$18.0^{+1.2}_{-1.1}$	−20.9	13^{+6}_{-5}	(19,23)

[a] In *F606W* filter.
[b] Synthetic AB magnitude.

Greiner et al. (2011) analysed the extinction along the line of sight through (undetected) host galaxies of 33 GRBs, nine of which are dark bursts. The values of A_V were obtained directly from observed SEDs of the afterglows (X-ray and optical). They found that a significant fraction of the bursts (25 per cent) have $A_V \sim 0.5$ mag and another 10 per cent have $A_V > 1$ mag. GRB 051008 with its $A_{V,\,\mathrm{LOS}} > 2$ mag is located in the 10 per cent of the bursts with high A_V (Zafar et al. 2011).

5.3 Conclusions

In this paper we gathered almost all available observations of the dark GRB 051008, including γ-ray and X-ray data, optical imaging and spectroscopy, NIR, and radio data. GRB 051008 is clearly an optically dark burst. No OA was detected for GRB 051008 to a limit of 23.3 mag within half an hour after the burst trigger, and the burst is dark in accordance with the darkness criteria of both Jakobsson et al. (2004) and van der Horst et al. (2009). We detected and studied the host galaxy of GRB 051008. It is a rather typical LBG located at the redshift of $z_{\mathrm{phot}} = 2.77^{+0.15}_{-0.20}$. The host galaxy has a SFR of $\sim 60\,\mathrm{M}_{\odot}\ \mathrm{yr}^{-1}$ typical for LBGs. The host is slightly younger and less dusty than LBGs with L^* luminosity, and it is almost 10 times less massive. It is one of the few cases where a GRB host has been found to be a classical LBG.

The redshift and the detection of GRB 051008 with Konus-*WIND* allowed us to calculate the isotropic-equivalent energy of the burst to be $E_{\mathrm{iso}} = (1.15 \pm 0.20) \times 10^{54}$ erg. This is a highly energetic long burst without detectable spectral lag and with a hard spectrum and rather early jet-break of $\sim$0.41 d determined from X-ray observations. The study of the host galaxy infers the presence of additional line-of-sight extinction towards the burst source. This extinction cannot be explained by the bulk extinction in the host galaxy, which is only moderate. Most probably it is produced by a dense circumburst medium.

We furthermore found the photometric redshift of nearby galaxies, and among them the two galaxies have a redshift $z \sim 2.8$, coinciding with the redshift of the host within statistical uncertainties. Therefore, the host may be situated in a gravitationally bound system. The redshift of all three galaxies is determined due to the presence of a clear and strong Lyman break feature.

ACKNOWLEDGEMENTS

We are grateful to S.N. Dodonov, T.A. Fatkhullin, M.V. Barkov, O.V. Egorov, M. Salvato, D.I. Karasyov, and V.A. Kolesnikov for useful discussions. AAV, ASP and PYuM were supported by the program 'Origin, structure, and evolution of objects in the Universe' funded by the Russian Academy of Sciences and RFBR grants 12-02-01336-a, 13-01-92204-Mong, 14-02-10015-K.

JG and AJC-T were supported by the Spanish programs ESP2005-07714-C03-03, AYA2007-63677, AYA2008-03467/ESP, and AYA2009-14000-C03-01. The data presented in this paper have been acquired using the ALFOSC camera, which is owned by the Instituto de Astrofísica de Andalucía (IAA) and operated at the Nordic Optical Telescope under the agreement between IAA and NBIfAFG of the Astronomical Observatory of Copenhagen. The Konus-*WIND* experiment is partially supported by a Russian Space Agency contract, RFBR grants 12-02-00032a and 13-02-12017 ofi-m.

DAK and SK acknowledge financial support by DFG grants Kl 766/13-2 and Kl 766/16-1. DAK acknowledges financial support by MPE and TLS.

Support for DAP is provided by NASA through Hubble Fellowship grant HST-HF-51296.01-A awarded by the Space Telescope Science Institute, which is operated for NASA by the Association of Universities for Research in Astronomy, Inc., under contract NAS 5-26555. This work made use of data supplied by the UK Swift Science Data Centre at the University of Leicester.

REFERENCES

Abazajian K. N. et al., 2009, ApJS, 182, 543
Amati L., 2006, MNRAS, 372, 233
Aptekar R. L. et al., 1995, Space Sci. Rev., 71, 265
Arnaud K. A., 1996, in Jacoby G., Barnes J., eds, ASP Conf. Ser. Vol. 101, Astronomical Data Analysis Software and Systems V. Astron. Soc. Pac., San Francisco, p. 17
Arnouts S., Cristiani S., Moscardini L., Matarrese S., Lucchin F., Fontana A., Giallongo E., 1999, MNRAS, 310, 540
Band D. L., 1997, ApJ, 486, 928
Band D. et al., 1993, ApJ, 413, 281
Beloborodov A. M., Stern B. E., Svensson R., 2000, ApJ, 535, 158
Beuermann K. et al., 1999, A&A, 352, L26
Bloom J. S., Frail A. D., Sari R., 2001, AJ 121, 2879
Bloom J. S., Kulkarni S. R., Djorgovski S. G., 2002, AJ, 123, 1111
Bloom J. S., Berger E., Kulkarni S. R., Djorgovski S. G., Frail D. A., 2003, AJ, 125, 999
Breeveld A., Marshall F., Blustin A., 2005, GCN Circ. No. 4079
Burrows D. N., Hill J. E., Nousek J. A., 2005, Space Sci. Rev., 120, 165
Butler N. R., 2007, AJ, 133, 1027
Calzetti D., Armus L., Bohlin R. C., Kinney A. L., Koornneef J., Storchi-Bergmann T., 2000, ApJ, 533, 682
Cameron P. B., 2005, GCN Circ. No. 4074
Castro-Tirado A. J. et al., 2007, A&A, 475, 101
Castro-Tirado A. J. et al., 2010, A&A, 517, A61
Cenko S. B. et al., 2009, ApJ, 693, 1484
Chandra P., Frail D. A., 2012, ApJ, 746, 156
Chen H.-W. et al., 2010, ApJ, 723, L218
Chevalier R. A., Li Z.-Y., 2000, ApJ, 536, 195
Devyatkin A. V., Gorshanov D. L., Kouprianov V. V., Verestchagina I. A., 2010, Solar System Res., 44, 68
Djorgovski S. G., Frail D. A., Kulkarni S. R., Bloom J. S., Odewahn S. C., Diercks A., 2001, ApJ, 562, 654
Elíasdóttir Á. et al., 2009, ApJ, 697, 1725
Evans P. A. et al., 2009, MNRAS, 397, 1177
Evans P. A. et al., 2010, A&A, 519, A102
Ferrero P., Klose S., 2005, GCN Circ. No. 4076
Ferrero P., Klose S., Kann A., Zeh A., Stecklum B., 2005, GCN Circ. No. 4085
Fioc M., Rocca-Volmerange B., 1997, A&A 326, 950
Fitzpatrick E. L., 1986, AJ, 92, 1068
Frail D. A., Kulkarni S. R., Berger E., Wieringa M. H., 2003, AJ, 125, 2299
Fynbo J. U. et al., 2001, A&A, 369, 373
Fynbo J. P. U., Prochaska J. X., Sommer-Larsen J., Dessauges-Zavadsky M., Mller P., 2008, ApJ, 683, 321
Fynbo J. P. U. et al., 2009, ApJS, 185, 526
Galama T., Wijers R. A. M., 2001, ApJ, 549, L209
Gehrels N. et al., 2004, ApJ, 611, 1005
Ghirlanda G., Ghisellini G., Lazzati D., 2004, ApJ, 616, 331
Gorosabel J. et al., 2003, A&A, 400, 127
Greiner J. et al., 2009, ApJ, 639, 1610
Greiner J. et al., 2011, A&A, 526, A30
Greiner J. et al., 2013, A&A, 560, A70
Grupe D., Nousek J. A., vanden Berk D. E., Roming P. W. A., Burrows D. N., Godet O., Osborne J., Gehrels N., 2007, AJ, 133, 2216
Hakkila J. et al., 2007, ApJS, 169, 62
Hashimoto T. et al., 2010, ApJ, 719, 378
Holland S. T. et al., 2010, ApJ, 717, 223

Hunt L., Palazzi E., Rossi A., Savaglio S., Cresci G., Klose S., Michalowski M., Pian E., 2011, ApJ, 736, L36
Ilbert O. et al., 2006, A&A, 457, 841
Jakobsson P., Hjorth J., Fynbo J. P. U., Watson D., Pedersen K., Bjrnsson G., Gorosabel J., 2004, ApJ, 617, L21
Jakobsson P. et al., 2005a, MNRAS, 362, 245
Jakobsson P. et al., 2005b, ApJ, 629, 45
Jakobsson P. et al., 2012, ApJ, 752, 62
Jaunsen A. O. et al., 2008, ApJ, 681, 453
Jimenez R., Piran T., 2013, ApJ, 773, id. 126
Kaneko Y., Preece R. D., Briggs M. S., Paciesas W. S., Meegan C. A., Band D. L., 2006, ApJS, 166, 298
Kennicutt R. C., 1998, ARA&A, 36, 189
Klose S., Hoegner C., 2005, GCN Circ. No. 4072
Krühler T. et al., 2011, A&A, 534, A108
Krühler T. et al., 2012a, ApJ, 758, 46
Krühler T. et al., 2012b, A&A, 546, A8
Küpcü Yoldaş A., Greiner J., Klose S., Krhler T., Savaglio S., 2010, A&A, 515, L2
Lamb D. Q., Reichart D. E., 2000, ApJ, 536, 1
Lazzati D., Covino S., Ghisellini G., 2002, MNRAS, 330, 583
Levan A. et al., 2006, ApJ, 647, 471
Liang E.-W., Racusin J. L., Zhang B., Zhang B.-B., Burrows D. N., 2008, ApJ, 675, 528
Liang E.-W., Lü H.-J., Hou S.-J., Zhang B.-B., Zhang B., 2009, ApJ, 707, 328
Malesani D., Kruehler T., Perley D., Fynbo J. P. U., Xu D., Milvang-Jensen B., Goldoni P., Schulze S., 2013, GCN Circ. No. 14225.
Margutti R. et al., 2013, MNRAS, 428, 729
Marshall F., Barthelmy S., Cummings J., Norris J., Perri M., Sakamoto T., 2005, GCN Circ. No. 4069
Mazets E. P. et al., 2001, in Costa E., Frontera F., Hjorth J., eds, Gamma-Ray Bursts in the Afterglow Era: Proceedings of the International Workshop Held in Rome, Italy, 17–20 October 2000, ESO Astrophysics Symposia. Springer-Verlag, p. 9
Melandri A. et al., 2008, ApJ, 686, 1209
Melandri A. et al., 2012, MNRAS, 421, 1265
Minaev P., Pozanenko A., Grebenev S., Molkov S., 2013, EAS Publ. Ser., 61, 75
Minaev P., Pozanenko A., Grebenev S., Molkov S., 2014, Astron. Lett., 40, 271
Norris J. P., Marani G. F., Bonnell J. T., 2000, ApJ, 534, 248
Nousek J. A. et al., 2006, ApJ, 642, 389
Odewahn S. C. et al., 1998, ApJ, 509, L5
Ohno M. et al., 2005, GCN Circ. No. 4297
Oke J. B. et al., 1995, PASP, 107, 375
Paczynski B., 1998, ApJ, 494, L45
Pérez-Ramírez D. et al., 2010, A&A, 510, 105
Perley D. A., Perley R. A., 2013, ApJ, 778, id. 172
Perley D. A. et al., 2009, AJ, 138, 1690
Perley D. A. et al., 2011, AJ, 141, 36
Perley D. A. et al., 2013, ApJ, 778, id. 128
Perri M., Capalbi M., Burrows D. N., 2005, GCN Circ. No. 4071
Piro L. et al., 2002, ApJ, 577, 680
Pozanenko A. S., Loznikov V. M., 2000, in Kippen R. M., Mallozzi R. S., Fishman G. J., eds, Gamma-ray Bursts, 5th Huntsville Symposium. AIP Conf. Ser. 526, Am. Inst. Phys., New York, p. 220
Pozanenko A. et al., 2007, Izvestiya Crymskoi Astrof. Obs., 103, 48
Prévot M. L., Lequeux J., Prévot L., Maurice E., Rocca-Volmerange B., 1984, A&A, 132, 389
Racusin J. L. et al., 2009, ApJ, 698, 43
Roming P. W. A. et al., 2005a, Space Sci. Rev., 120, 95
Roming P., Marshall F., Blustin A., 2005b, GCN Circ. No. 4070
Rossi A. et al., 2012, A&A, 545, A77
Rumyantsev V., Biryukov V., Pozanenko A., 2005, GCN Circ. No. 4081
Sari R., Piran T., Narayan R., 1998, ApJ, 497, L17
Sari R., Piran T., Halpern J. P., 1999, ApJ, 519, L17
Savaglio S., Glazebrook K., Le Borgne D., 2009, ApJ, 691, 182
Schlegel D. J., Finkbeiner D. P., Davis M., 1998, ApJ, 500, 525
Shapely A. E., Steidel C. C., Adelberger K. L., Dickinson M., Giavalisco M., Pettini M., 2001, ApJ, 562, 95
Svensson K. M. et al., 2012, MNRAS, 421, 25
Tanvir N. R. et al., 2008, MNRAS, 388, 1743
Taylor G. B., Frail D. A., Kulkarni S. R., Shepherd D. S., Feroci M., Frontera F., 1998, ApJ, 502, L115
Thöne C. C. et al., 2013, MNRAS, 428, 3590
Tinney C., Stathakis R., Cannon R., Galama T. J., 1998, IAU Circ. 6896
Ukwatta T. N. et al., 2010, ApJ, 711, 1073
Ulanov M. V., Golenetskii S. V., Frederiks D. D., Mazets R. L., Aptekar E. P., Kokomov A. A., Palshin V. D., 2005, Nuovo Cimento C, 28, 351
van der Horst A. J., Kouveliotou C., Gehrels N., Wijers R. A. M. J., Cannizzo J. K., Racusin J., Burrows D. N., 2009, ApJ, 699, 1087
Volnova A. A. et al., 2010a, Astrophys. Bull., 65, 334
Volnova A. A. et al., 2010b, in McEnery J. E., Racusin J. L., Gehrels N., eds, Gamma Ray Bursts. AIP Conf. Proc. 1358, Greenbelt, Annapolis, MD
von Kienlin A. et al., 2003, A&A, 411, L299
Wright E. L., 2006, PASP, 118, 1711
Xin L. P. et al., 2010, MNRAS, 401, 2005
Zafar T., Watson D., Fynbo J.P.U., Malesani D., Jakobsson P., de Ugarte Postigo A., A&A, 532, id. A143
Zauderer B. A. et al., 2013, ApJ, 767, 161
Zeh A., Klose S., Hartmann D. H., 2004, ApJ, 609, 952
Zhang B., Fan Y. Z., Dyks J., Kobayashi S., Mszros P., Burrows D. N., Nousek J. A., Gehrels N., 2006, ApJ, 642, 354
Zhang B. et al., 2007, ApJ, 655, 989

This paper has been typeset from a TEX/LATEX file prepared by the author.